

Coherent acceleration of Bose-Einstein condensates

Sierk Pötting^{1,2,3 *}, Marcus Cramer^{1,4}, Christian H. Schwalb^{1,4}, Han Pu¹, and Pierre Meystre¹

¹*Optical Sciences Center, University of Arizona, Tucson, Arizona 85721*

²*Max-Planck-Institut für Quantenoptik, 85748 Garching, Germany*

³*Sektion Physik, Universität München, 80333 München, Germany*

⁴*Fachbereich Physik der Philipps-Universität, Marburg, Germany*

(October 25, 2018)

We present a theoretical analysis of the coherent acceleration of atomic Bose-Einstein condensates. A first scheme relies on the ‘conveyor belt’ provided by a frequency-chirped optical lattice. For potentials shallow enough that the condensate is not fragmented, the acceleration can be interpreted in terms of sequential Bragg scattering, with the atomic sample undergoing transitions to a succession of discrete momentum sidemodes. The narrow momentum width of these sidemodes offers the possibility to accelerate an ultracold atomic sample such as e.g. a Bose-Einstein condensate without change in its momentum distribution. This is in contrast to classical point particles, for which this kind of acceleration leads to a substantial heating of the sample. A second scheme is based on the idea of a synchronous particle accelerator consisting of a spatial array of quadrupole traps. Pulsing the trapping potential creates a traveling trap that confines and accelerates the atomic system. We study this process using the concept of phase stability.

PACS numbers: 03.75.Fi, 32.80.-t, 42.50.Vk

I. INTRODUCTION

A number of applications of atom optics, from inertial sensors [1] to nanofabrication, atomic holography [2–4] and certain schemes for quantum computation [5,6], can benefit substantially from manipulating quantum degenerate atomic beams with finely controlled potentials. In particular, the atomic de Broglie wavelength can be easily modified by accelerating or decelerating an atomic beam to the appropriate velocity, thereby making it a tunable source. There is also an increased need to control ultracold samples of atoms in confined geometries, as e.g. in atomic waveguides for potential integrated atom optics applications. First transport experiments in waveguides were recently carried out with non-condensed atomic samples, both in stationary and in time-dependent potentials [7–10].

The simplest and most important coherence property of an atomic beam is its monochromaticity. With this in mind, our goal in this paper is to determine the extent to which it is possible to significantly accelerate an initially

quasi-monochromatic atomic sample without losing this property. For this purpose it is sufficient to describe the atomic system in the Hartree mean-field limit, remembering that this “classical-like” description makes implicit assumptions on the quantum statistical properties of the Schrödinger field, essentially assuming that it is in a coherent state. Other, more subtle aspects of the quantum coherence of accelerated matter-wave fields [11–14] will be addressed in future work.

We consider two different acceleration schemes: in the first one, an accelerated trap is provided by a frequency-chirped optical lattice, while in the second one we consider a synchronous accelerator consisting of a spatial array of quadrupole traps, which is similar to a scheme that was successful in manipulating the velocity of neutral molecules and atoms [15,16]. We restrict our discussion to one dimension for simplicity.

Ultracold atoms in both static and time-dependent optical lattices have been investigated in several contexts in the recent past. At the single-atom level, they were exploited extensively in theoretical and experimental work aiming at demonstrating effects such as Bloch oscillations [17–19], Landau-Zener tunneling [20,21], the appearance of Wannier-Stark ladders [20,22–24], quantum chaos [25] and the dynamics of mesoscopic quantum superpositions [26]. The extension of this work to Bose-Einstein condensates [27,28] includes the first demonstration of a mode-locked atom laser [29], a device that can also be interpreted in terms of Landau-Zener tunneling. Bragg scattering of Bose-Einstein condensates off a periodic optical potential was also used in experiments to characterize their coherence and phase properties [30,31]. It was exploited to generate multiple momentum sidemodes of the condensate used in matter-wave four-wave mixing experiments [32–34] and to realize atomic beam splitters used in coherent matter-wave amplifiers [35,36].

Of particular relevance in the present context is Ref. [19], which explicitly considers the acceleration of atoms in a moving periodic potential and interprets it in terms of momentum transfer via multiple adiabatic rapid passage. This reference also reports experiments demonstrating the acceleration of atomic molasses with large initial momentum spreads as well as of ensembles with subrecoil momentum distributions. The final momentum spread is limited by the lattice recoil energy for the broad samples and by the initial distribution for the subrecoil atoms, see Figs. 11 and 13 of Ref. [19]. We

*email: sierk.potting@wotan.opt-sci.arizona.edu

will show that we can suppress heating even in the case the atomic temperature is substantially lower than the recoil temperature associated with the lattice, which in particular holds for a Bose-Einstein condensate and its quasi-monochromatic momentum distribution.¹

The paper is organized as follows: Section II investigates the acceleration of an ultracold atomic ensemble in a frequency-chirped optical lattice. We set the stage by first considering an ensemble of *classical* point particles spread over a large number of lattice periods. We compare its dynamics to that of a Bose-Einstein condensate of the same spatial extent, described in the Hartree mean-field regime. We demonstrate that while the accelerated classical particles undergo considerable heating, which is however substantially eliminated by the quantum interferences associated with the extended atomic wave functions of ultracold samples. The quantum dynamics are interpreted as continuous Bragg scattering in a lattice with time-dependent detuning. We briefly review the formalism of Bragg scattering within the framework of a partitioned momentum space *et al.* [38], which allows one to discuss the acceleration in terms of a coupled-mode approach that leads to a determination of optimum acceleration parameters. We conclude this section by some comments on the role of the mean-field interaction. Section III then turns to the synchronous acceleration scheme. Again, we first consider the acceleration of non-interacting classical point particles, this time using the concept of phase stability. We then study numerically the acceleration of a condensate. Finally, section IV is a conclusion and outlook.

II. ACCELERATED OPTICAL LATTICE

A. Classical acceleration

To set the stage for our discussion, we first consider the acceleration of an ensemble of non-interacting, point-like classical particles in a frequency-chirped optical lattice formed by two counterpropagating laser beams. The resulting time-dependent optical potential is

$$V(z, t) = V_0 \cos[K(t)z - \delta(t)t], \quad (1)$$

where

$$K(t) = k_{\rightarrow}(t) + k_{\leftarrow}(t) \quad (2)$$

is the sum of the instantaneous wave numbers of the left- and right-propagating laser fields forming the lattice, and

$$\delta(t) = \omega_{\rightarrow}(t) - \omega_{\leftarrow}(t) = c[k_{\rightarrow}(t) - k_{\leftarrow}(t)] \quad (3)$$

is the instantaneous frequency detuning between them. The instantaneous phase velocity of the lattice fringes is therefore

$$v_{\text{lat}}(t) = \frac{\partial}{\partial t} \left(\frac{\delta(t)t}{K(t)} \right) \quad (4)$$

which reduces to the usual phase velocity δ/K in the case of constant detuning. Assuming that v_{lat} remains much less than the velocity of light c at all times we have

$$k_{\rightarrow}(t) - k_{\leftarrow}(t) \ll k_{\rightarrow}(t) + k_{\leftarrow}(t), \quad (5)$$

and it is an excellent approximation to set $k_{\rightarrow}(t) + k_{\leftarrow}(t) \approx 2k_L$, where k_L is a nominal laser wave number independent of time. The potential (1) reduces then to

$$V(z, t) \approx V_0 \cos[2k_L z - \delta(t)t] \quad (6)$$

and

$$v_{\text{lat}}(t) \approx \left(\frac{1}{2k_L} \right) \frac{\partial[\delta(t)t]}{\partial t} \quad (7)$$

where the time derivative is the instantaneous frequency of the field. While we have shown numerically that this is not necessarily an optimum choice, we restrict our analysis in this paper to linear accelerations produced by a time-dependent detuning of the form

$$\delta(t) = \eta t, \quad (8)$$

producing a lattice group velocity

$$v_{\text{lat}}(t) = \eta t / k_L \quad (9)$$

and a constant acceleration $a_{\text{lat}} = \eta/k_L$. This simple case is sufficient to identify and discuss the major physical mechanisms at play in the acceleration of the atoms.

To determine the dynamics of an ensemble of classical point particles on this lattice, we have numerically solved Newton's equations of motion for a large number of atoms initially at rest at random points in an interval large compared to the lattice period. The size of this interval and the probability of finding an atom at a given point were chosen to mimic the shape of a Bose-Einstein condensate density profile, to which we turn shortly.

The solid lines in Figs. 1 and 2 show the evolution of the mean position $\langle z(t) \rangle$ and mean velocity $\langle v(t) \rangle$ of the classical atomic ensemble over the acceleration time for two values of a_{lat} . We observe that the mean atomic velocity is always somewhat less than the instantaneous lattice velocity v_{lat} , the dashed line in Fig. 2. The cause of this difference is revealed in Fig. 3, which shows the momentum distribution of the classical ensemble $n(k)$ at a fixed time t and for the same two values of a_{lat} , where we expressed the momentum p in terms of the wavenumber $k = p/\hbar$. In addition to peaks at positive momenta

¹Shortly after submission of this work, this prediction was independently confirmed in experiments on the acceleration of a condensate by a frequency-chirped optical lattice [37].

indicative of accelerated atoms that contribute to an increase in the mean velocity of the sample, a significant group of particles acquire negative momenta, i.e. they are accelerated in the direction opposite to the lattice motion. These are atoms that spill into a well to their left in the moving potential. A similar effect will also be encountered in the synchronous particle accelerator of section III.

Another important feature of Fig. 3 is that the momentum distributions of both the accelerated and decelerated groups of atoms are rather wide. This shows that (even ignoring the decelerated atoms), the lattice accelerator produces a considerable heating of the atomic sample. This can potentially be a very serious problem for applications requiring a high degree of spatial coherence of the atomic beam. Surprisingly perhaps, we will see that the situation can be significantly improved in the quantum regime, a result of quantum interferences.

B. Condensate acceleration

We now turn to the acceleration of a Bose–Einstein condensate at temperature $T = 0$. For the present study, it is sufficient to describe its dynamics in a Hartree mean-field approximation via the Gross-Pitaevskii equation for the normalized condensate wave function $\Psi(z, t)$,

$$i\hbar \frac{\partial}{\partial t} \Psi(z, t) = \left[-\frac{\hbar^2}{2m} \frac{\partial^2}{\partial z^2} + V_0 \cos[2k_L z - \delta(t)t] \right] \Psi(z, t) + NU_0 |\Psi|^2 \Psi(z, t), \quad (10)$$

where N is the number of atoms in the condensate. For the reduction to one dimension we assume the condensate to be in its transverse ground state $u_g(\mathbf{r}_\perp)$. This is accounted for by the effective nonlinear parameter U_0 ,

$$U_0 = \frac{4\pi\hbar^2 a_s}{m} \int d\mathbf{r}_\perp |u_g(\mathbf{r}_\perp)|^4, \quad (11)$$

where a_s is the s -wave scattering length.

In the presence of a periodic potential, one needs to beware of the possible fragmentation of the condensate via a Mott insulator transition. This problem has been investigated in Ref. [39], which discusses the transition to this phase from the superfluid phase as a function of the ratio κ between the depth of the optical lattice and the inter-well tunneling matrix element. The first Mott transition, corresponding to an occupation of one atom per lattice site, occurs for $\kappa \approx 5.8z$, z being the number of nearest neighbors [39], corresponding typically to lattice potential depths of the order of 2.5-5 lattice recoil energies. Here we consider only situations where the lattice potential is shallow enough that such fragmentation does not occur.

We solve Eq. (10) numerically using a split-operator technique for a condensate of the same initial density profile as the classical ensemble considered earlier. The

resulting mean position $\langle z(t) \rangle$ and mean velocity $\langle v(t) \rangle$ of the condensate are shown by the dotted lines in Figs. 1 and 2. We observe that whereas the displacement dynamics is very similar to the classical case, the mean velocity exhibits two differences. First, the condensate shows pronounced time-dependent oscillations, the well-known Bloch oscillations. Second, the higher of the two lattice accelerations causes $\langle v \rangle$ to saturate to a constant value, an effect due to increased Landau-Zener tunneling.²

The difference between the classical and quantum situations is evidenced even more strikingly in Fig. 4. Instead of being composed of two broad continua as in Fig. 3, the condensate momentum distribution $\phi(k)$, which is the Fourier transform of the spatial wavefunction $\Psi(z)$, consists of a series of very narrow peaks located at integer multiples of $2k_L$.³ Physically, this is due to the fact that while the classical particles probe the local value of the lattice potential, the ultracold Bose-Einstein condensate probes a region of the lattice comprising a large number of maxima and minima, and hence its full periodicity. As such, the individual classical particles are channeled in one or the other potential well of the time-dependent potential, while the ultracold atoms are diffracted by it. Their dynamics is governed by the quantum interferences that give rise to Bragg scattering, with the resulting narrow peaks of Fig. 4. This is a central result of this paper: it shows that after acceleration, the ultracold atoms can still be largely monochromatic. The next section takes advantage of the physical difference in physics between the acceleration of quantum and semiclassical samples to investigate ways to achieve this goal.

C. Sequential Bragg resonances

With atom interferometric applications in mind, we call an acceleration scheme ideal if it leaves all atomic population in one single momentum mode whose value is determined by the velocity v_{lat} of the optical lattice. We can therefore define a figure of merit of the accelerator as one minus the fraction of atoms in other momentum side-modes. Fig. 4 suggests that we have to restrict ourselves to certain acceleration rates and times in order not to lose too many atoms. The closest we were able to approach

²Superfluid effects are not an issue in our system: The critical velocity for typical Bose–Einstein condensates was recently determined to lie in the mm/s regime [40–42], much less than the velocities to which the condensate is accelerated. For the acceleration rates under consideration here, the instantaneous lattice velocity exceeds the critical velocity already after a small fraction of the total acceleration time.

³The experiment of Ref. [37] shows clear evidence of such peaks.

“perfect” acceleration with our simple linear acceleration scheme is the example of Fig. 4(a).

In the following we consider a simple coupled-mode description of the acceleration process to identify the important parameters in its optimization. We neglect the effects of the mean-field energy for now and extend the case of a static lattice as shown in Ref. [38] to accelerated ones. Starting from the collisionless form of the Gross-Pitaevskii equation (10) and introducing the momentum space condensate wave function that we already used in Fig. 4

$$\phi(k, t) = \frac{1}{\sqrt{2\pi}} \int_{-\infty}^{\infty} dz \psi(z, t) e^{-ikz}, \quad (12)$$

one finds readily that its evolution is governed by the coupled difference-differential equations

$$i\hbar \frac{\partial}{\partial t} \phi(k) = \frac{\hbar^2 k^2}{2m} \phi(k) + \frac{V_0}{2} \left[\phi(k - 2k_L) e^{-i\eta t^2} + \phi(k + 2k_L) e^{i\eta t^2} \right]. \quad (13)$$

From these equations, it is clear that states with momentum k only couple to neighboring states with $k = \pm 2k_L$. Thus we can partition the momentum space into intervals of width $2k_L$ and substitute for $\phi(k, t)$ a set of wave functions restricted to these intervals,

$$\phi_n(k) = \phi(k) \quad \text{for} \quad (n-1)k_L < k \leq (n+1)k_L. \quad (14)$$

The partitioned wave functions ϕ_n are then expressed in terms of the shifted momentum $q = k - 2nk_L$ and multiplied with an interval-dependent phase factor,

$$\phi_n(q) = \phi_n(k) e^{-i\eta t^2}. \quad (15)$$

Finally, we use the numerically established property that each of these partial wave functions suffers a momentum spread small compared to the mode spacing, see Fig 4, to approximate them by plane waves at $q = 0$,

$$\phi_n(q = 0, t) = c_n(t). \quad (16)$$

In units of the lattice recoil frequency $\omega_{\text{rec}} = 2\hbar k_L^2/m$, we introduce the dimensionless variables

$$\tau = t\omega_{\text{rec}}, \quad \tilde{\eta} = \eta/\omega_{\text{rec}}^2, \quad \tilde{V}_0 = V_0/\hbar\omega_{\text{rec}}, \quad (17)$$

in terms of which the equation of motion Eq. (13) can be rewritten in matrix form as

$$i \frac{\partial}{\partial \tau} \mathbf{c}(\tau) = V(\tau) \mathbf{c}(\tau), \quad (18)$$

where we defined the vector of coefficients — which essentially gives the probability amplitudes for the various momentum sidemodes — as

$$\mathbf{c}(\tau) = (\cdots, c_{-1}, c_0, c_1, \cdots)^T \quad (19)$$

and the coupling matrix $V(\tau)$ is given by

$$V(\tau) = \begin{pmatrix} \ddots & \ddots & 0 & & & \\ \ddots & \omega_{-1}(\tau) & \frac{\tilde{V}_0}{2} & 0 & & \\ 0 & \frac{\tilde{V}_0}{2} & \omega_0(\tau) & \frac{\tilde{V}_0}{2} & 0 & \\ & 0 & \frac{\tilde{V}_0}{2} & \omega_1(\tau) & \ddots & \\ & & 0 & \ddots & \ddots & \end{pmatrix}. \quad (20)$$

The diagonal elements of $V(\tau)$ are responsible for the time-dependence of the coupling matrix and are given by

$$\omega_n(\tau) = n^2 - 2n\tilde{\eta}\tau. \quad (21)$$

Finally, we can define the detuning Δ_n between adjacent modes as

$$\Delta_n(\tau) = \omega_n(\tau) - \omega_{n-1}(\tau) = 2n - 2\tilde{\eta}\tau - 1. \quad (22)$$

Equation (18) describes Bragg scattering of atoms off the periodic optical lattice. Bragg resonances occur whenever one of the detunings $\Delta_n(\tau)$ becomes equal to zero. From Eq. (22), we observe that these detunings depend both on the scattering order n and on time, this latter dependence resulting from the acceleration of the optical potential. As a result of the linear acceleration, neighboring pairs of modes are therefore successively moved in and out of resonance, so that in contrast to the case of classical particles, the physical process underlying the atomic acceleration are successively tuned and detuned Bragg resonances.⁴

This sequence of resonances is illustrated in Fig. 5, which shows the evolution of the population dynamics of a few momentum sidemodes of the condensate. The solid lines give the results of a truncated coupled-modes analysis, while the dotted curves show the results of the direct solution of the Gross-Pitaevskii equation, in which case the various sidemode populations are calculated from

$$|c_n(\tau)|^2 = \int_{(2n-1)k_L}^{(2n+1)k_L} dk |\phi(k, \tau)|^2. \quad (23)$$

The two approaches are in excellent agreement, despite the fact that the coupled-mode analysis included only eight modes in the present example. The upper graph clearly illustrates the sequential population transfer towards sidemodes of higher momentum. The lower graph focuses on the first side mode of negative momentum. After initial oscillations, indicative of its coupling to other

⁴Ref. [19] refers to this process as “multiple adiabatic rapid passage,” an equally appropriate terminology.

modes, its population stabilizes to a final value resulting from the fact that it is then far-off resonance from any other mode.

D. Optimal acceleration

Having identified sequential Bragg resonances as the physical mechanism of acceleration of ultracold atoms, we can now attempt to optimize the external parameters to achieve maximum velocity and figure of merit of the accelerator. Ignoring for now all but the two adjacent modes c_n and c_{n-1} , we observe that they couple with a time-dependent Rabi frequency Ω_n given by

$$\Omega_n(\tau) = \frac{1}{4} \sqrt{\tilde{V}_0^2 + \Delta_n^2(\tau)}. \quad (24)$$

We can gain some insight into the time scale of this coupling mechanism by introducing an averaged Rabi frequency $\bar{\Omega}$ over the interval $\tau_R = 1/\bar{\eta}$, the time it takes the system to move from one Bragg resonance to the next, see Eq. (22),

$$\bar{\Omega} = \frac{1}{\tau_R} \int_{\tau_n}^{\tau_n + \tau_R} d\tau \Omega_n(\tau), \quad (25)$$

where $\tau_n = (n-1)/\bar{\eta}$. Note that $\bar{\Omega}$ is independent of the index n . Hence, one can expect that a close to optimal mode-to-mode coupling should correspond to

$$\bar{\Omega}\tau_R \approx \pi, \quad (26)$$

since in this case the system can complete half of an averaged Rabi cycle in the time it takes to move from one Bragg resonance to the next. The complete population of one mode is then approximately transferred to the next mode, thereby increasing the momentum of the condensate by $2\hbar k_L$. If the lattice acceleration is too fast for this Rabi transfer to fully occur, lower momentum modes remain significantly populated. This is the case in the example of Fig. 4(b). Conversely, atoms accelerated too slowly undergo more than one half Rabi cycle between two modes. This results in oscillations in the expectation values $\langle v \rangle$ and $\langle z \rangle$.

We have mentioned in the context of Fig. 5(b) that once a momentum sidemode is shifted out of resonance, its population remains constant. This accounts for the saturation in $\langle v \rangle$ shown in Fig. 2. In contrast to the classical case where all atoms that are captured in a potential well remain captured, here, in the quantum regime, atoms initially accelerated may gradually be moved out of resonance, after which they retain a constant velocity.

Fig. 6 summarizes the results of a numerical optimization of the lattice acceleration rate. It confirms that if the acceleration rate is too large one can only transfer a small fraction of the population to the next mode, while

if it is too small we couple to modes with negative momentum, as manifested in the small dip in all curves near the origin. The plateau-like feature defines the regime of efficient coupling, where around 85% of the population is transferred.

We mention that it is also possible to accelerate the condensate by applying a series of Bragg pulses, each of them resonant with the next higher pair of momentum modes. For the specific parameters used in our figures, one could then reach accelerations approximately twice as high as in the case of continuous detuning, but further improvement would require stronger Bragg pulses that create additional couplings to different modes [38]. We do not go into further details about this approach here. Rather, future work will implement learning algorithms to determine ideal chirping and/or pulse sequences to achieve the coherent and lossless acceleration of ultracold atomic samples.

We conclude this section by remarking that so far, we have ignored the effects of the mean-field energy on the Bragg acceleration of the atomic sample. But it should be expected that the associated nonlinear phase shifts can effect it significantly. This is illustrated in Fig. 7, where we plot the temporal evolution of the zeroth momentum sidemode for different mean-field energies (atomic numbers). For large mean-field energies we observe that the local evolution can deviate significantly from the low-density limit, although the general behavior is similar. For the Sodium parameter used in our simulations, we find that in condensates of up to 10^5 atoms the nonlinear effects are small enough that the system obeys the predictions of the simplified linear model.

III. SYNCHRONOUS PARTICLE ACCELERATION

We now turn to our second accelerator scheme, which uses a time-varying conservative potential well, formed, e.g., by external magnetic fields. The idea is to initially place the condensate near the top of a potential well. As it moves down the well, it gains kinetic energy at the expense of its potential energy. If the external field is turned off precisely when the atoms are near the potential minimum, then the condensate will wind up with an increased kinetic energy. The process can be repeated by letting the condensate pass through a sequence of pulsed potential wells appropriately displaced in space and time. It can thus gain a considerable amount of kinetic energy.

We first discuss how such a method can be used to accelerate an ensemble of classical particles. Fig. 8 illustrates the potential energy, $V(z)$, as a function of particle position. In analogy to the concepts of charged particle accelerators, we express the atomic position in terms of a ‘‘phase angle’’ ϕ , with a periodicity of $2L$. Two examples of potentials are depicted in Fig. 8: a sinusoidal potential and a chained harmonic one. The potential maxima

occur at $\phi = -\pi/2 + 2n\pi$ ($n = 0, \pm 1, \pm 2, \dots$), while the minima are at $\phi = \pi/2 + 2n\pi$. Now suppose a particle initially located near the potential maximum accelerates to the potential minimum for a time τ , at which moment the original potential is switched off and a new set of potential wells identical to the previous ones, but with a phase shift of π , is switched on. Then the particle will find itself again near the top of the potential well, and continue to be accelerated.

In order to describe quantitatively this acceleration scheme, it is convenient to introduce the concept of the *synchronous particle*. This is a particle that travels exactly the distance L (or π in terms of phase angle) during the time interval τ . We denote its phase and velocity right after the switching by ϕ_s and v_s , respectively. By definition, then, the initial phase ϕ_s of the synchronous particle remains unchanged.

The kinetic energy gained by the synchronous particle during one acceleration stage is given by

$$\Delta E_K(\phi_s) \equiv V(\phi_s) - V(\phi_s + \pi). \quad (27)$$

We can regard this increase as originating from a continuously acting, average force [15]

$$F(\phi_s) = \Delta E_K(\phi_s)/L.$$

Consider now a non-synchronous particle with initial phase $\phi = \Delta\phi + \phi_s$ and velocity $v = \Delta v + v_s$. Its motion relative to the synchronous particle is governed approximately by the equation of motion

$$\frac{d^2}{dt^2} \Delta\phi = \frac{\pi}{mL} [F(\phi_s + \Delta\phi) - F(\phi_s)]. \quad (28)$$

Depending on the initial conditions, Eq. (28) describes either stable or unstable dynamics of the motion of a collection of particles. It is easy to see that for stable acceleration, we must have

$$-\pi/2 \leq \phi_s \leq 0.$$

Fig. 9 plots the phase stability diagram for the two potentials depicted in Fig. 8, obtained by numerically solving Eq. (28). For a given ϕ_s , the closed curve depicts the boundary of a “bucket”, inside of which a stable acceleration is achieved. Since $\Delta E_K(\phi_s)$ decreases from $2V_0$ to 0 when ϕ_s changes from $-\pi/2$ to 0, we see there is always a trade-off between fast acceleration and large bucket size, i.e., large acceptance. Furthermore, for $-\pi/2 < \phi_s < -\pi/12$, the chained harmonic potential gives a larger bucket compared to the sinusoidal potential.

To test our scheme on a condensate, we have solved the time-dependent Gross-Pitaevskii equation (10) with the time-dependent potential of Fig. 8. Our results are illustrated in Fig. 10, which shows the velocity of the condensate at each of the switching times of the external fields, for both harmonic and sinusoidal potentials. The

switching is chosen to occur at the moment the center of mass of the condensate travels a distance L . For this calculation, we choose the initial wave function to be a Gaussian centered at $\phi_0 = -\pi/6$ with a width of $0.1L$. The inserts in the figure show the normalization of the wave function, which characterizes the loss of atoms during their acceleration. This is calculated by discarding the atoms leaked outside of the well that traps the center of the mass of the condensate. Less loss is observed for the harmonic potential than for the sinusoidal one, a result of the larger bucket size in the former case (see Fig. 9). We also observe a weaker influence of the condensate mean-field energy in the case of a harmonic potential. However, while atomic collisions do increase the losses and decrease acceleration rates, their effect is not very dramatic, a result similar to that already encountered with the chirped lattice accelerator. In addition, we checked the momentum distribution of the wave function during the acceleration and found no significant variations of the momentum width, hence, monochromaticity is also preserved in this scheme.

The solid line in Fig. 10 gives the velocity of a classical particle under the action of a continuous and constant force $F(\phi_0) = \Delta E_K(\phi_0)/L$. As the figure shows, the average acceleration a of the condensate can indeed be approximated by $a = F(\phi_0)/m$.

We finally note that in the case of alkali atoms, an acceleration of $\sim 10^5$ m/s² requires a well depth of 10 mK and width $L = 100$ μ m is needed. In view of current advances in the technology of magnetic microtraps [43], these numbers should not pose as an unsurmountable challenge for experimentalists.

IV. SUMMARY AND CONCLUSION

In conclusion, we demonstrated two coherent mechanisms to accelerate Bose–Einstein condensates with very little atom loss while preserving its monochromaticity. The first mechanism, based on the use of an accelerated optical lattice, can be interpreted as resulting from a sequence of Bragg resonances, which can lead to a remarkable preservation of the monochromaticity of the atomic sample under appropriate conditions. This analysis enabled us to identify an optimal regime of acceleration rates for reasonable experimental parameters. The second scheme uses a time-varying potential analogous to those used in the synchronous acceleration of charged particle. Acceleration is achieved by switching on and off the potential in an appropriate way such that the condensate keeps gaining kinetic energy at the expense of its potential energy. In contrast to the first scheme where only quasi–discrete modes are populated, here the momentum of the condensate evolves continuously.

In future work, it will be important to optimize the time-dependence of the accelerators, so as to achieve a factor of merit as close to unity as possible. We propose

to approach this problem using genetic learning algorithm techniques. It will also be necessary to go past the mean-field theory in order to determine the higher-order coherence properties of the accelerated beams, in particular their atom statistics. In addition, these acceleration devices are potentially important to generate non-classical matter wave fields to be used in improving the signal to noise ratio in future atom optical sensors. The discrete set of momentum sidemodes that are macroscopically excited in the sequential Bragg resonances make this problem particularly well suited for quantum optical “essential modes” approaches familiar from quantum nonlinear optics.

ACKNOWLEDGMENTS

This work is supported in part by the U.S. Office of Naval Research under Contract No. 14-91-J1205, by the National Science Foundation under Grant No. PHY98-01099, by the U.S. Army Research Office, and by the Joint Services Optics Program.

-
- [1] T. L. Gustavson, P. Bouyer, and M. A. Kasevich, *Phys. Rev. Lett.* **78**, 2046 (1997).
- [2] J. Fujita, S. Mitake, and F. Shimizu, *Phys. Rev. Lett.* **84**, 4027 (2000).
- [3] A. Soroko, *J. Phys. B* **30**, 5621 (1997).
- [4] O. Zobay, E. V. Goldstein, and P. Meystre, *Phys. Rev. A* **60**, 3999 (1999).
- [5] D. Jaksch, H.-J. Briegel, J. I. Cirac, C. W. Gardiner, and P. Zoller, *Phys. Rev. Lett.* **82**, 1975 (1999).
- [6] G. K. Brennen, C. M. Caves, P. S. Jessen, and I. H. Deutsch, *Phys. Rev. Lett.* **82**, 1060 (1999).
- [7] D. Müller, D. Z. Anderson, R. J. Grow, P. D. D. Schwindt, and E. A. Cornell, *Phys. Rev. Lett.* **83**, 5194 (1999).
- [8] M. Key, I. G. Hughes, W. Rooijakkers, B. E. Sauer, E. A. Hinds, D. J. Richardson, and P. G. Kazansky, *Phys. Rev. Lett.* **84**, 1371 (2000).
- [9] N. H. Dekker, C. S. Lee, V. Lorent, J. H. Thywissen, S. P. Smith, M. Drndić, R. M. Westervelt, and M. Prentiss, *Phys. Rev. Lett.* **84**, 1124 (2000).
- [10] W. Hänsel, J. Reichel, P. Hommelhoff, and T. W. Hänsch, *Phys. Rev. Lett.* **86**, 608 (2001).
- [11] E. V. Goldstein and P. Meystre, *Phys. Rev. Lett.* **80**, 5036 (1998).
- [12] E. V. Goldstein, O. Zobay, and P. Meystre, *Phys. Rev. A* **58**, 2373 (1998).
- [13] G. A. Prataiviera, E. V. Goldstein, and P. Meystre, *Phys. Rev. A* **60**, 4846 (1999).
- [14] P. Meystre, *Atom Optics*, Springer Verlag, New York (2001), in press.
- [15] H. L. Bethlem, G. Berden, A. J. A. van Roij, F. M. H. Crompvoets, and G. Meijer, *Phys. Rev. Lett.* **84**, 5744 (2000).
- [16] J. A. Maddi, T. P. Dinneen, and H. Gould, *Phys. Rev. A* **60**, 3882 (1999); H. Bethlem, G. Berden, and G. Meijer, *Phys. Rev. Lett.* **83**, 1558 (1999); H. Bethlem, G. Berden, F. M. H. Crompvoets, R. T. Jongma, A. J. A. van Roij, and G. Meijer, *Nature* **406**, 491 (2000).
- [17] M. B. Dahan, E. Peik, J. Reichel, Y. Castin, and C. Salomon, *Phys. Rev. Lett.* **76**, 4508 (1996).
- [18] E. Peik, M. Ben Dahan, I. Bouchoule, Y. Castin, and C. Salomon, *Appl. Phys. B* **65**, 685 (1997).
- [19] E. Peik, M. B. Dahan, I. Bouchoule, Y. Castin, and C. Salomon, *Phys. Rev. A* **55**, 2989 (1997).
- [20] Q. Niu, X.-G. Zhao, G. A. Georgakis, and M. G. Raizen, *Phys. Rev. Lett.* **76**, 4504 (1996).
- [21] C. F. Bharucha, K. W. Madison, P. R. Morrow, S. R. Wilkinson, B. Sundaram, and M. G. Raizen, *Phys. Rev. A* **55**, R857 (1997).
- [22] S. R. Wilkinson, C. F. Bharucha, K. W. Madison, Q. Niu, and M. G. Raizen, *Phys. Rev. Lett.* **76**, 4512 (1996).
- [23] K. W. Madison, C. F. Bharucha, P. R. Morrow, S. R. Wilkinson, Q. Niu, B. Sundaram, and M. G. Raizen, *Appl. Phys. B* **65**, 693 (1997).
- [24] J. Zapata, A. M. Guzman, M. G. Moore, and P. Meystre, *Phys. Rev. A* **63**, 023607 (2001).
- [25] W. H. Oskay, D. A. Steck, B. G. Klappauf, and M. G. Raizen, *Laser Phys.* **9**, 265 (1999).
- [26] D. L. Haycock, P. M. Alsing, I. H. Deutsch, J. Grondalski, and P. S. Jessen, *Phys. Rev. Lett.* **85**, 3365 (2000).
- [27] K. Berg-Sørensen and K. Mølmer, *Phys. Rev. A* **58**, 1480 (1998).
- [28] D.-I. Choi and Q. Niu, *Phys. Rev. Lett.* **82** 2022 (1999).
- [29] B. P. Anderson and M. A. Kasevich, *Science* **282**, 1686 (1998).
- [30] J. Stenger, S. Inouye, A. P. Chikkatur, D. M. Stamper-Kurn, D. E. Pritchard, and W. Ketterle, *Phys. Rev. Lett.* **82**, 4569 (1999).
- [31] E. W. Hagley, L. Deng, M. Kozuma, M. Trippenbach, Y. B. Band, M. Edwards, M. Doery, P. S. Julienne, K. Helmerson, S. L. Rolston, and W. D. Phillips, *Phys. Rev. Lett.* **83**, 3112 (1999).
- [32] L. Deng, E. W. Hagley, J. Wen, M. Trippenbach, Y. B. Band, P. S. Julienne, J. E. Simsarian, K. Helmerson, S. L. Rolston, and W. D. Phillips, *Nature* **398**, 218 (1999).
- [33] E. V. Goldstein and P. Meystre, *Phys. Rev. A* **59**, 3896 (1999).
- [34] M. Trippenbach, Y. B. Band, P. S. Julienne, *Phys. Rev. A* **62**, 023608 (2000).
- [35] S. Inouye, T. Pfau, S. Gupta, A. P. Chikkatur, A. Görlitz, D. E. Pritchard, and W. Ketterle, *Nature* **402**, 641 (1999).
- [36] M. Kozuma, L. Deng, E. W. Hagley, J. Wen, R. Lutwak, K. Helmerson, S. L. Rolston, and W. D. Phillips, *Phys. Rev. Lett.* **82**, 871 (1999).
- [37] O. Morsch, J. H. Müller, M. Cristiani, and E. Arimondo, eprint cond-mat/0103466.
- [38] P. B. Blakie and R. J. Ballagh, *J. Phys. B: At. Mol. Opt. Phys.* **33**, 3961 (2000).
- [39] D. Jaksch, C. Bruder, J. I. Cirac, C. W. Gardiner, and

- P. Zoller, Phys. Rev. Lett. **81**, 3108 (1998).
- [40] C. Raman, M. Köhl, R. Onofrio, D. S. Durfee, C. E. Kuklewicz, Z. Hadzibabic, and W. Ketterle, Phys. Rev. Lett. **83**, 2502 (1999).
- [41] R. Onofrio, C. Raman, J. M. Vogels, J. R. Abo-Shaeer, A. P. Chikkatur, and W. Ketterle, Phys. Rev. Lett. **85**, 2228 (2000).
- [42] S. Burger, F. S. Cataliotti, C. Fort, F. Minardi, M. Inguscio, M. L. Chiofalo, and M. P. Tosi, to appear in Phys. Rev. Lett. **86**, 14 May (2001).
- [43] J. Reichel, W. Hänsel, P. Hommelhoff, and T. W. Hänsch, Appl. Phys. B **72**, 81 (2001).

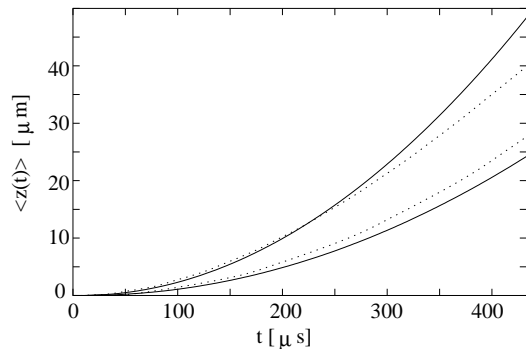


FIG. 1. Mean displacement of the atomic cloud: The simulation uses 10^5 Sodium atoms initially at rest with a Gaussian spatial distribution of longitudinal width $50 \mu\text{m}$ and transverse width $5 \mu\text{m}$. The laser wavelength is $\lambda_L = 985 \text{ nm}$ and the lattice depth V_0 is chosen to be half the lattice recoil energy. The Sodium mass is $m = 3.82 \cdot 10^{-26} \text{ kg}$ and the s-wave scattering length $a_s = 4.9 \text{ nm}$. Two upper curves: $a_{\text{lat}} = 724.1 \text{ ms}^{-2}$. Two lower curves: $a_{\text{lat}} = 327.8 \text{ ms}^{-2}$. Solid lines: classical particles, dotted lines: BEC. Unless otherwise stated, the same parameters are used through Fig. 7.

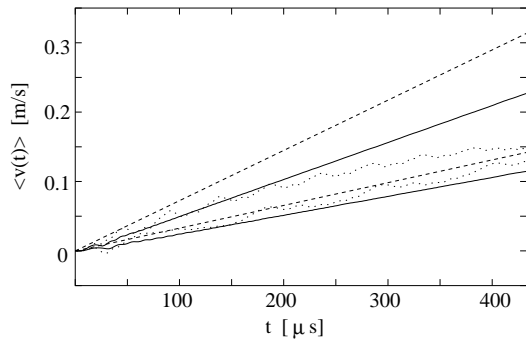


FIG. 2. Mean velocity of the atomic cloud: $a_{\text{lat}} = 724.1 \text{ ms}^{-2}$ (three upper curves), $a_{\text{lat}} = 327.8 \text{ ms}^{-2}$ (three lower curves). Solid lines: classical particles; dotted lines: BEC; dashed lines: instantaneous lattice velocity.

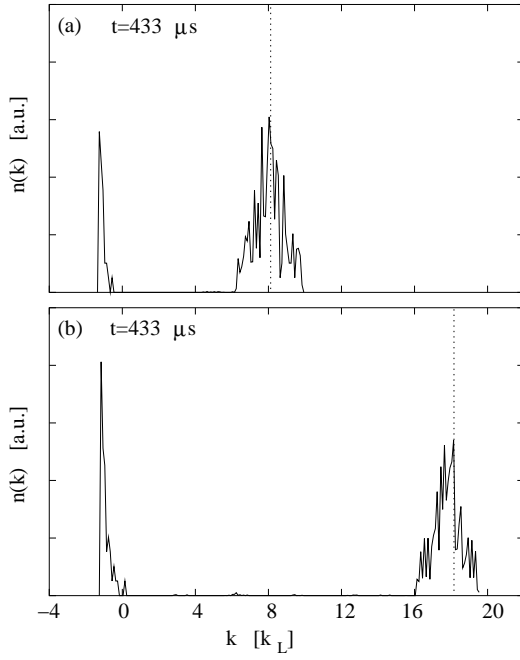


FIG. 3. Momentum distribution $n(k)$ of an ensemble of 10^5 classical particles for $a_{\text{lat}}=(\text{a}) 327.8 \text{ ms}^{-2}$, (b) 724.1 ms^{-2} , in units of k_L . Vertical dotted line: instantaneous lattice momentum at time of plot.

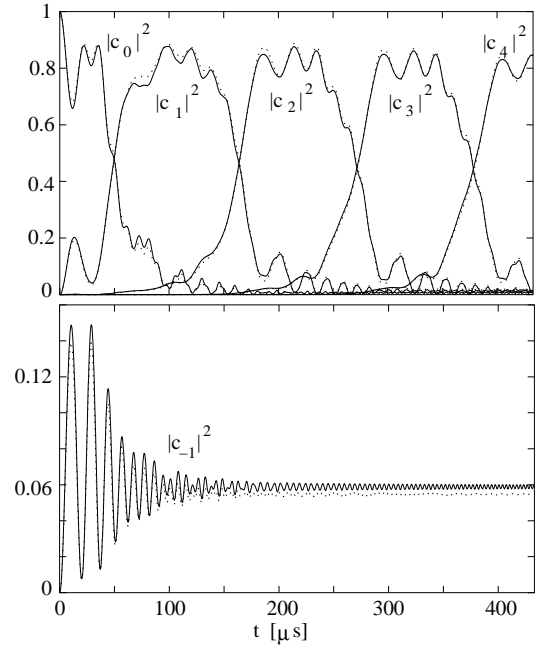


FIG. 5. Temporal evolution of the mode population for an acceleration of 327.8 ms^{-2} . Upper graph: $n = 0$ to $n = 4$ modes. Lower graph: $n = -1$ mode. Solid line: solution of truncated coupled-mode equations; dotted line: direct solution of the Gross-Pitaevskii equation.

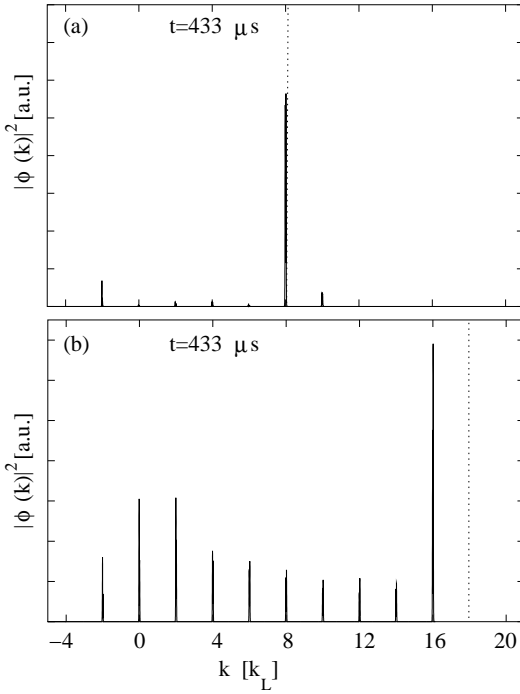


FIG. 4. Momentum distribution $\phi(k)$ of a Bose-Einstein condensate of 10^5 atoms for $a_{\text{lat}}=(\text{a}) 327.8 \text{ ms}^{-2}$, (b) 724.1 ms^{-2} , in units of k_L . Vertical dotted line: instantaneous lattice momentum at time of plot.

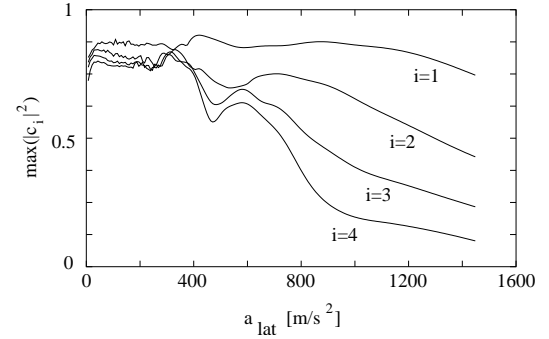


FIG. 6. Maximum population of the i th mode as a function of acceleration, obtained from the truncated coupled-mode equations.

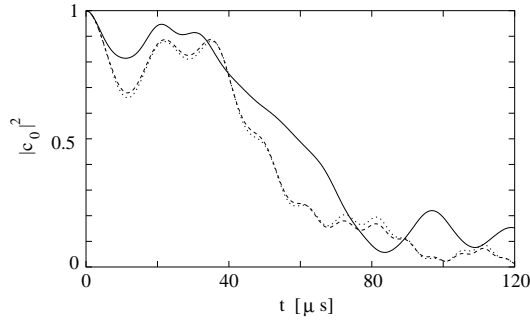


FIG. 7. Population of the zeroth momentum mode for 10^6 (solid), 10^5 (dotted) and 10^4 atoms (dashed) in the condensate, obtained from a simulation of the full Gross-Pitaevskii equation for an acceleration $a_{\text{lat}} = (a) 327.8 \text{ ms}^{-2}$.

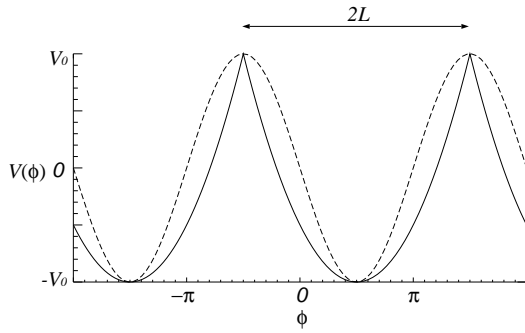


FIG. 8. Potential energy as a function of phase angle. The dashed line represents a sinusoidal potential, the solid line represents a chained harmonic potential. For both cases, the well depth is $2V_0$.

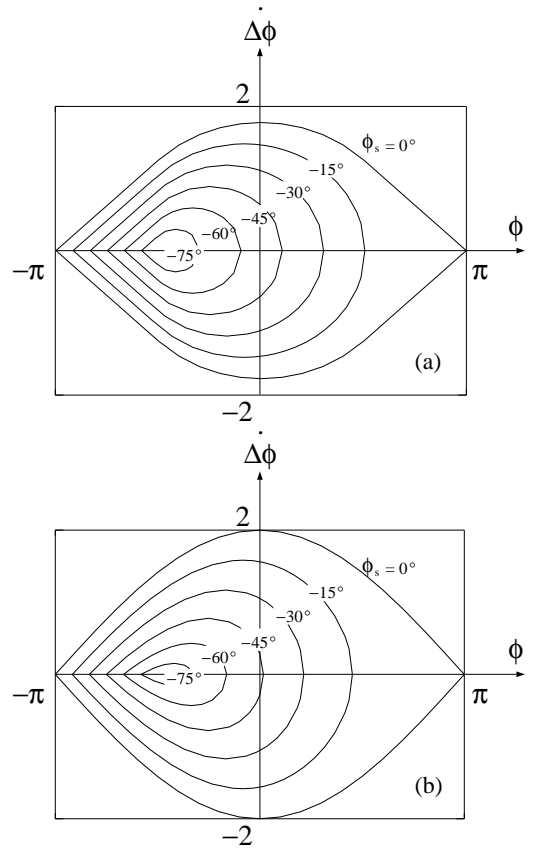


FIG. 9. Phase stability diagram for various values of ϕ_s for (a) the harmonic potential and (b) the sinusoidal potential. The unit for $\Delta\dot{\phi}$ is $\sqrt{2\pi V_0}/(mL^2)$.

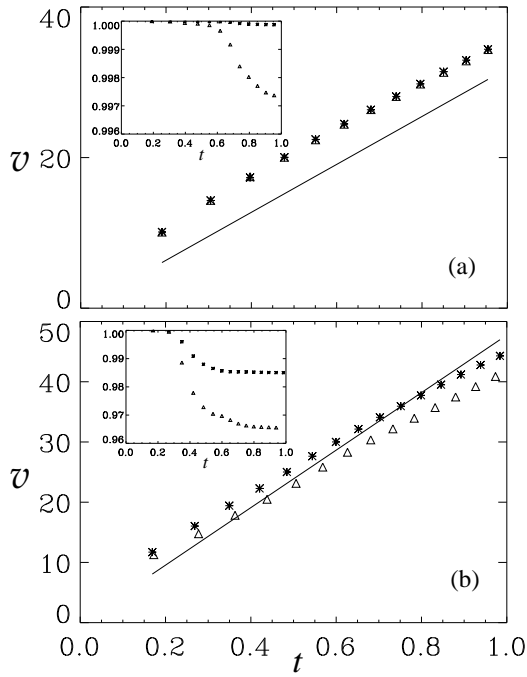


FIG. 10. Condensate velocity at the times of the successive switchings for (a) the harmonic potential and (b) the sinusoidal potential. Stars: non-interacting condensate with $U = 0$; triangles: interacting condensate with $U = 10$. For practical choices of parameters, the typical value for U in our dimensionless units is on the order of 1 to 10. Insets: normalization of the wavepackets. Time in units of $2mL^2/(\hbar\pi^2)$, velocity in units of $\hbar\pi/(mL)$, and energies in units of $\hbar^2\pi^2/(2mL^2)$. In this example, $V_0 = 150$. (In practice, V_0 should have a much larger value for realistic choices of parameters. However, in our calculations large values of V_0 gives rise to too much numerical noise.)